JOCES/2012/117705

LIPID PHOSPHATE PHOSPHATASE 3 PARTICIPATES IN TRANSPORT CARRIER FORMATION AND PROTEIN TRAFFICKING IN THE EARLY SECRETORY PATHWAY

Enric Gutiérrez-Martínez[*,†], Inés Fernández-Ulibarri[*,§], Francisco Lázaro-Diéguez[*,¶], Ludger Johannes[ǂ], Susan Pyne[#], Elisabet Sarri[*], and Gustavo Egea[*,†,@]

[*]Departament de Biologia Cel·lular, Immunologia i Neurociències, Facultat de Medicina, Universitat de Barcelona, Barcelona (Spain); [†]Instituts d'Investigació Biomèdica August Pi I Sunyer (IDIBAPS) and Nanociència i Nanotecnologia (IN^{2}UB), Barcelona (Spain); [ǂ]Institute Curie, CNRS-UMR 144, 75005 Paris (France); [#]Cell Biology Group, Strathclyde Institute of Pharmacy and Biomedical Science, University of Strathclyde, Glasgow (United Kingdom).

[§]Current address: Helmholtz-University Group Oncolytic Adenoviruses, DKFZ German Cancer Research Center, Heidelberg University Hospital, 69120 Heidelberg (Germany).

[¶]Current address: Department of Developmental and Molecular Biology, Albert Einstein College of Medicine, The Bronx, 10461 New York (USA).

Running title: LPP3 function in the secretory pathway

Keywords: diacylglycerol, phosphatidic acid phosphatase, Golgi apparatus, ERGIC, Endoplasmic reticulum, lipid homeostasis

Abbreviations: DAG, diacylglycerol; DOG, 1,2-dioctanoyl-sn-glycerol; ERES, Endoplasmic reticulum exit sites; ERGIC, endoplasmic reticulum-Golgi intermediate compartment; LPP, lipid phosphate phosphatase; PAP, phosphatidic acid phosphatase; STxB, Shiga toxin subunit B.

@Corresponding author: Department de Biologia Cel·lular, Immunologia i Neurociències, Facultat de Medicina, Universitat de Barcelona, c/ Casanova 143, 08036 Barcelona (Spain). Phone: (+)34.93.402.19.09; e-mail: gegea@ub.edu.

JCS Advance Online Article. Posted on 16 April 2013

SUMMARY

The inhibition of phosphatidic acid phosphatase (PAP) activity by propanolol indicated that diacylglycerol (DAG) is required for the formation of transport carriers at the Golgi and for retrograde trafficking to the ER (Fernández-Ulibarri et al. 2007, Mol. Biol. Cell 18, 3250-3263). We here report that the PAP2 family member lipid phosphate phosphatase 3 (LPP3, also known as PAP2b) localizes in compartments of the secretory pathway from ERES to the Golgi complex. The depletion of human LPP3: (i) reduces the number of tubules generated from the ERGIC and the Golgi, with those formed from the Golgi being longer in LPP3-silenced cells than in control cells; (ii) impairs the Rab6-dependent retrograde transport of Shiga toxin subunit B from the Golgi to the ER, but not the anterograde transport of VSV-G or ssDsRed; and (iii) induces a high accumulation of Golgi-associated membrane buds. LPP3 depletion also reduces *de novo* synthesized DAG and the Golgi-associated DAG contents. Remarkably, the overexpression of a catalytically inactive form of LPP3 mimics the effects of LPP3 knockdown on Rab6-dependent retrograde transport. We conclude that LPP3 participates in the formation of retrograde transport carriers at the ER/Golgi interface, where it transitorily cycles, and during its route to the plasma membrane.

INTRODUCTION

The Golgi complex is involved in the processing, sorting and transport of membrane components (lipids and proteins) to appropriate subcellular destinations, and is also a membranous platform for signaling, metabolic and cytoskeleton proteins. Transport to and from the Golgi complex is mediated by transport carriers (vesicles and/or tubules) which are generated in sequential stages beginning with the formation of a bud, followed by its elongation, constriction, and final fission. These different stages require tight control of membrane deformations by a complex molecular machinery composed of coat proteins, motors and protein domains that bend membranes (Krauss et al., 2008; Roux et al., 2005; Sorre et al., 2009), and lipid components that recruit cytosolic proteins, modulate protein functions and modify the architecture and physical properties of the membrane bilayer (Bard and Malhotra, 2006; Burger, 2000; Huijbregts et al., 2000; Kooijman et al., 2005; Lippincott-Schwartz and Phair, 2010; Shemesh et al., 2003; van Meer et al., 2008). Membrane curvature is facilitated by conical lipid molecules such as lysophosphatidic acid (LPA), phosphatidic acid (PA) and diacylglycerol (DAG).

DAG has a dual role in the formation of carriers since it acts as a scaffold and activator of proteins involved in signaling and membrane fission such as PKD and ArfGAP1 (Baron and Malhotra, 2002; Fernandez-Ulibarri et al., 2007), and it also facilitates negative curvature. Moreover, there is a constant and relatively large pool of DAG in Golgi membranes (Lev, 2006). For all these reasons, DAG has been extensively associated with vesicular transport events at the Golgi in yeast and mammalian cells (Asp et al., 2009; Baron and Malhotra, 2002; Fernandez-Ulibarri et al., 2007; Kearns et al., 1997; Litvak et al., 2005; Sarri et al., 2011). Nonetheless, PA has recently been reported to regulate transport carrier formation at the Golgi (Yang et al., 2008 and 2011).

DAG at the Golgi is tightly regulated by metabolic pathways that affect its consumption and production. On the one hand, CDP-cholinephosphotransferase (CPT) consumes DAG to generate phosphatidylcholine (PC) (Henneberry et al., 2002; Sarri et al., 2011; Tian et al., 2008) and diacylglycerol kinase (DAGK) converts DAG into PA (Merida et al., 2008; Nagaya et al., 2002). On the other hand, DAG is generated by sphingomyelin synthases (SMSs) that convert PC and ceramide into sphingomyelin (SM) and DAG (Subathra et al., 2011; Villani et al., 2008), and by the sequential coupling of

phospholipase D (PLD) and phosphatidic acid phosphatases (PAPs) in which the former generates PC-derived PA, which in turn is dephosphorylated by the latter to DAG (Roth, 2008; Sciorra and Morris, 1999).

Two types of mammalian PAPs have been identified according to their subcellular localization, substrate affinities and regulatory mechanisms (Brindley et al., 2009; Grimsey et al., 2008; Pyne et al., 2005; Sigal et al., 2005). PAP1 enzymes are cytoplasmic, Mg^{2+}-dependent and inhibited by N-ethylmaleimide, and PA is their only known substrate. PAP2 enzymes are integral membrane proteins, Mg^{2+}-independent, and insensitive to N-ethymaleimide. PAP2 are also known as lipid phosphate phosphatases (LPPs) because, in addition to PA, they can also catalyze *in vitro* the dephosphorylation of other lipid phosphates such as ceramide-1-phosphate (C1P), sphingosine-1-phosphate (S1P), and lysophosphatidic acid (LPA) with different affinities (PA ~ LPA > C1P > S1P) (Long et al., 2005; Roberts et al., 1998; Waggoner et al., 1996). Due to the crucial role of the substrates and products of PAP activity in cell signaling, several PAP isoforms have been shown to contribute to the production of lipid signaling metabolites both inside and outside cells (Brindley and Pilquil, 2009; Pyne et al., 2009).

In mammals, three LPP isoforms have been reported: LPP1 (PAP2a), LPP2 (PAP2c) and LPP3 (PAP2b). LPPs are glycoproteins with a channel-like structure containing six putative transmembrane domains. The catalytic site is arranged into three distinct conserved domains (C1-C3) and faces the extracellular side of the plasma membrane or the luminal side of endomembranes (Long et al., 2008; Zhang et al., 2000). This topology is important since lipid phosphates do not easily cross membranes and therefore, their access to LPPs, particularly in intracellular compartments, will be a major factor in their dephosphorylation rate and metabolism (Brindley and Pilquil, 2009). At present, the only experimental strategy to regulate a particular LPP isoform is by modulating its expression (Escalante-Alcalde et al., 2003; Kai et al., 1997; Long et al., 2008; Ulrix et al., 1998). All LPPs are present to some extent in the plasma membrane (Alderton et al., 2001; Jasinska et al., 1999; Kai et al., 2006), while LPP2 and LPP3 have been variably localized in endomembranes such as ER, endosomes, vesicular structures and the Golgi complex (Alderton et al., 2001; Morris et al., 2006; Sciorra and Morris, 1999). However, little is known about their role in these subcellular compartments. The use of propanolol, which inhibits general PAP activity (Pappu and Hauser, 1983), has indicated that the DAG generated in this reaction is involved in the

fission (Fernandez-Ulibarri et al., 2007) and in budding (Asp et al., 2009) at the Golgi complex, with the subsequent alteration in membrane trafficking at the ER/Golgi interface. Here we examine the molecular machinery involved in the production of DAG required for the membrane trafficking. We show that the PAP2 family member lipid phosphate phosphatase 3 (hereafter LPP3, also known as PAP2b) localizes in the early secretory pathway trafficking stations such as ERES, the ERGIC and the Golgi complex, mainly contributing to the retrograde transport.

RESULTS

LPP3 localizes in compartments of the secretory pathway

Single labeling experiments in HeLa cells with anti-LPP3 antibodies (Long et al., 2008) stained a Golgi-like perinuclear region and peripheral dot-like structures, overlapping with the endoplasmic reticulum-Golgi intermediate compartment (ERGIC) markers ERGIC53-GFP (Fig. 1A) and KDEL receptor (KDELr) (not shown). To assess the localization of LPP3 in more detail, cells were treated with the microtubule-depolymerizing agent nocodazole (NZ) and co-labeled for LPP3 and markers of several transport stations along the secretory pathway, such as Sec31A (endoplasmic reticulum exiting sites, ERES), KDELr (endoplasmic reticulum-Golgi intermediate compartment, ERGIC), GM130 (*cis*-Golgi), and Golgin97 (*trans*-Golgi/TGN). NZ treatment induces the formation of Golgi ministacks that, despite their small size, preserve the structural and molecular polarity (*cis*-to-*trans*) of the Golgi ribbon (Dejgaard et al., 2007; Ho et al., 1989), which in turn facilitates colocalization analysis. In NZ-treated cells, LPP3 overlapped with all these markers to a variable extent (Sec31A > KDELr > GM130 > Golgin 97) (Fig. 1B and C). Previous studies have reported LPP3 at the ER and the plasma membrane (Long et al., 2008; Sciorra and Morris, 1999), but with our anti-LPP3 antibodies the staining of both subcellular compartments (except for ERES) was not obvious. However, LPP3 was observed in both compartments after the expression of the human GFP-tagged LPP3 (hLPP3-GFP) in COS-7 and HeLa cells, in addition to its localization at the Golgi (Suppl. Fig. 1). The presence of LPP3 at ERES led us to examine its dynamics at the ER. To this end, COS-7 cells expressing hLPP3-GFP were examined by time-lapse confocal microscopy. They showed dot-like structures that exhibited slow, short range movements within ER cisterna, with no clear directionality (Fig. 1D and Suppl. movie 1). Sometimes, these dot-like structures jumped from one cisterna to another (Suppl. movie 1). This dynamic behavior is in accordance with what has been reported for ERES-associated transmembrane proteins (Hammond and Glick, 2000; Kano et. al., 2004).

A pool of LPP3 constitutively cycles between the ER and the Golgi, and behaves like an ERGIC-resident protein.

To examine the dynamics of LPP3 in the secretory pathway to the plasma membrane, we compared the ER-to-Golgi transport of LPP3 with that of a characteristic secretory

protein, the membrane-associated vesicular stomatitis virus glycoprotein G (VSV-G), using the fluorescence recovery after photobleaching (FRAP) technique at the Golgi area. VSV-G was induced to accumulate at the ER at 40°C overnight, and then cells were treated with cycloheximide and incubated for 15 min at 32 ºC, which allows VSV-G to reach the Golgi. At this point the Golgi-associated fluorescence was photobleached and its recovery was analyzed. After 30 min, most of the fluorescence at the ER was lost, while the initial Golgi-associated fluorescence intensity was recovered (Suppl. Fig. 2A). Conversely, in cells expressing hLPP3-GFP the fluorescence at the ER barely decreased despite the arrival of LPP3 at the Golgi. This difference could be explained if LPP3 were more stably associated with ER membranes than VSV-G, or if LPP3 were in part constitutively recycled back from the Golgi to the ER. To investigate this latter possibility, we bleached the fluorescence signal out of the Golgi area in COS-7 cells expressing hLPP3-GFP for 24 h and then added cycloheximide. After the photobleaching, we observed a partial recovery of the ER-associated signal (Suppl. Fig. 2B), which most likely have come from a pool of hLPP3-GFP located at the ERGIC and at the Golgi that is recycled back to the ER.

Collectively, these results strongly indicate that LPP3 behaves, in part, like an ERGIC-resident protein, cycling between the ER and the Golgi.

LPP3 participates in ERGIC membrane dynamics

As a first approach to examining the functional role of LPP3 in membrane trafficking at the ER/Golgi interphase, we used propranolol (an inhibitor of PAP activity; Billah et al., 1989) to assess its effect on the dynamics of ERGIC-53, a protein which constitutively cycles between the Golgi and the ER. HeLa cells expressing ERGIC53-GFP were incubated first at 15°C, which blocks both anterograde and retrograde protein transport from the ERGIC, resulting in the accumulation of recycling proteins in swollen peripheral ERGIC clusters (Klumperman et al., 1998; Saraste and Svensson, 1991). The cells were then rewarmed to 37°C. In agreement with previous reports (Ben-Tekaya et al., 2005), control cells showed numerous ERGIC53-GFP positive globular-like structures moving throughout the cytoplasm and forming transient tubular structures in a continuous process of elongation and shrinkage (Fig. 2A; Suppl. Movie 2). In contrast, propanolol-treated cells showed very few tubules emanating from ERGIC53-GFP structures (Fig. 2B; Suppl. movie 3), which were less motile than untreated cells

(compare suppl. movies 2 and 3). When propanolol was removed, ERGIC tubulation was re-established (Fig. 2C; suppl. movie 4).

We next studied the role of LPP3 in ERGIC- and Golgi-associated membrane dynamics and protein transport. For this purpose, we suppressed the expression of LPP3 by transient transfection of siRNAs and lentiviral infection with shRNAs in HeLa and Swiss 3T3 cells, respectively. In HeLa cells, two out of four different siRNAs against LPP3 exhibited a reduction in the protein level (about 70%) when added either individually or together (Fig. 3A). A similar decrease in LPP3 protein levels was also obtained in Swiss 3T3 cells (suppl. Fig. 3). As a proof of specificity, we show that our anti-LPP3 antibody recognizes the expressed form of the human FLAG-tagged LPP3, giving the same electrophoretic bands pattern as that given by the anti-FLAG antibody (Fig 3A).

To examine the effects of LPP3 silencing on the tubulation of the ERGIC, control and LPP3-knockdown HeLa cells were incubated at 15°C for 1 h and then shifted to 37°C, fixed and stained for KDELr (Fig. 3B). At 15°C, a large amount of KDELr-stained dot-like structures appeared dispersed throughout the cytoplasm in both control and LPP3-silenced cells (Fig. 3B). After rewarming, numerous tubules appeared in control cells, but their formation was reduced in silenced cells (Figs. 3B and C) as occurred in propanolol-treated cells (Fig. 2A). To investigate the link between the inhibitory effect of LPP3 depletion on the ERGIC tubulation and the decrease in the DAG pool (see below), we examined whether the reduction in ERGIC tubulation could be prevented by adding the short fatty acid chain diacylglycerol analogue 1,2-dioctanoyl-sn-glycerol (DOG). When added shortly before the rewarming of LPP3-silenced cells, DOG significantly recovered the tubulation of KDELr-associated dot-like structures (Fig. 3D, red arrows; Fig. 3E). Collectively, these results support the participation of LPP3 in ERGIC membrane dynamics.

LPP3 is not involved in the transport of anterograde cargo

To examine whether the effects on ERGIC dynamics of LPP3 depletion alter protein transport from the ER to the Golgi, we used two cargo markers: the transmembrane VSV-G and the soluble signal sequence-tagged DsRed (ssDsRed) proteins. HeLa cells constitutively expressing the thermosensitive mutant form (ts045) of the GFP-tagged VSV-G were transfected with oligonucleotides (#6 and #8) to silence the expression of LPP3. After 48 h, transfected cells were incubated overnight at 40°C to accumulate

VSV-G-GFP in the ER. Upon a shift to the permissive temperature (32°C), we analyzed the kinetics of acquisition of Endo H resistance, which is a hallmark of VSV-G transported to the *cis*/middle Golgi. The transport of VSV-G from the ER to the Golgi was not perturbed in LPP3-depleted cells (Fig. 4A). Next, we analyzed the ssDsRed transport from ERGIC peripheral clusters in control and LPP3-silenced HeLa cells that had been cotransfected with ERGIC53-GFP and ssDsRed. After blocking the transport from the ERGIC by incubating cells for 2 h at 15°C, ssDsRed mainly accumulated in enlarged peripheral punctated structures and in the Golgi in both control and LPP3-silenced cells (Fig. 4Ba and c). After 20 min of rewarming to 37°C (Fig. 4Bb and d; Fig. 4C), LPP3-silenced cells showed greater colocalization of ERGIC53-GFP peripheral punctated structures with the ssDsRed protein than control cells (compare magnified insets in Fig. 4Ce and f; Fig. 4D for quantitative analysis). However, the percentage of ssDsRed that colocalized with ERGIC53-GFP over the total ssDsRed-positive punctated structures remained unaltered between control and LPP3-silenced cells (Fig. 4E). This result indicates that the transport of ssDsRed from the ERGIC to the Golgi was not impaired by the depletion of LPP3. Moreover, we observed a decrease in the density of ERGIC53-GFP punctated structures in LPP3-silenced cells (compare ERGIC53-GFP panels c and d in Fig. 4C; Fig. 4F for quantitative analysis), which was in turn accompanied by an increase in their average size (compare magnified insets in Fig. 4e and f; Fig. 4G for quantitative analysis). Similar results were observed in cells cultured at 37°C, showing a significant decrease in the density of endogenous KDELr dot-like structures in LPP3-silenced cells respect to control cells (Suppl. Fig. 4). Collectively these results indicate that LPP3 participates in the maintenance of the architecture and dynamics of the ERGIC, but not in the anterograde transport of membrane and luminal cargo.

LPP3 participates in the retrograde protein transport

Previous reports indicate that incubation of cells at 15°C induces the formation of tubules enriched in Golgi-associated SNAREs (Gos28 and GS15) and Rab (Rab6) proteins (Martinez-Alonso et al., 2007). As in our examination of the membrane tubulation from the ERGIC, here we first studied the formation of Rab6-GFP tubular and vesicular transport carriers in control and propanolol-treated cells by live imaging (suppl. Fig. 5). After 1 h at 15°C, control cells showed a large number of tubular and vesicular Rab6-containing structures connected to the Golgi and dispersed throughout

the cytoplasm. To study the dynamics of Rab6-GFP transport carriers formed at 15°C, cells were then rewarmed to 37°C. In control cells, there was a fast consumption of previously formed Rab6-GFP tubules in small vesicles and a fast formation of new thin, short tubular structures. Some of these tubules were distributed throughout the cytoplasm and were moving rapidly towards the cell periphery, whereas others emerged directly from the Golgi (Suppl. Fig. 5 and movie 5). Propanolol-treated cells showed a decrease in the rate of newly formed Rab6-GFP transport carriers exiting the Golgi, but they were more extended, and remained so for a longer time before their total disruption into small vesicular structures (Suppl. Fig. 5 and movie 6). Next, we examined the morphology and density of newly generated Rab6-GFP transport carriers (tubules and vesicles) from Golgi membranes in control and LPP3-silenced HeLa cells stably expressing Rab6-GFP, which, as before, had first been cooled to 15°C for 1 h and then shifted to 37°C. After 10 min of rewarming, LPP3-depleted cells showed fewer Rab6-GFP particles than control cells (compare panels b and d in Fig. 5A; Fig. 5B for quantitative analysis). Interestingly, although LPP3-silenced cells contained fewer tubules (Fig. 5C), they were longer than those in control cells (arrows in magnified boxes from panels b and d in Fig. 5A, Fig; 5D for quantitative analysis). Collectively, these results indicate that LPP3 participates in the formation of Rab6-GFP transport carriers generated at the Golgi.

To further investigate the role of LPP3 in Rab6-dependent protein transport, we analyzed the trafficking of the cy3-tagged subunit B of the Shiga toxin (STxB), which is transported from the Golgi to the ER in a COPI-independent and Rab6-dependent manner (White et al., 1999). Control and LPP3 silenced cells stably expressing Rab6-GFP were incubated with STxB at 4°C for 30 min (Suppl. Fig. 6a and d), washed to remove unbound STxB and then shifted to 37°C to initiate the internalization of the toxin. After 2 h at 37°C, STxB was mostly seen at the Golgi (Suppl. Fig. 6b and e). When cells were subsequently incubated at 15°C for 60 min, STxB appeared in enlarged peripheral vesicular structures, with the concomitant loss of the Golgi staining (Suppl. Fig. 6c and f). At 15°C, we could barely see STxB colocalizing with Rab6-GFP (data not shown), in agreement with previous reports demonstrating that Golgi-emerging tubules formed at low temperature lack cargo (Martinez-Alonso et al., 2007). When cells were rewarmed to 37°C for 10 min STxB reached the ER in about 50% of control cells, which was assessed by visualization of the characteristic reticular and nuclear envelope ring patterns stained with cy3-STxB (Fig. 5Ea, red arrows).

Conversely, in LPP3-silenced cells most STxB remained in the peripheral vesicle-like structures (Fig.5Ec; Fig.5F for quantitative analysis). In control cells, Rab6-GFP tubules contained STxB (Fig. 5Eb and magnified boxes). Taking into account that at 15°C the STxB was barely present in tubular structures, we conclude that most of these tubules containing STxB and Rab6-GFP were newly-formed during the rewarming to 37°C. Conversely, in most of LPP3-silenced cells, colabeled tubules were almost absent (Fig. 5Ed and magnified boxes), which is consistent with the reduction of Rab6-GFP tubular structures caused by LPP3 depletion (Fig. 5C).

To ensure that the observed trafficking defects caused by LPP3-silencing did not represent off-target effects of siRNA transfection, we performed rescue experiments involving murine LPP3, which lacks complementation for human siRNA sequences, and its protein expression levels are not perturbed (Fig. 4A). Remarkably, expression of this siRNA-resistant myc-tagged murine LPP3 protein reversed the blockade of the STxB arrival at the ER (Fig. 5G, asterisks).

Finally, we examined whether COPI-dependent retrograde transport is also regulated by LPP3. To this end, we monitored the transport of STxB containing the KDEL sequence in its COOH-terminus (STxB-KDEL) (Johannes et al., 1997). When STxB-KDEL reaches the ER compartment, it is retained, showing an ER-like staining pattern. Control and LPP3-silenced Swiss 3T3 cells were incubated with cy3-STxB-KDEL at 19°C to accumulate the toxin in early endosomes. Subsequently, cells were shifted to 37°C to synchronize the toxin transport first to the Golgi and then to the ER, which in control cells occurred in 6 h (Supp. Fig. 7). In contrast, at this time STxB-KDEL was still accumulated in the Golgi of LPP3 silenced cells (Suppl Fig. 7). Taken together, these results indicate that LPP3 is involved in both COPI-dependent and COPI-independent (Rab6-dependent) transport from the Golgi to the ER.

A catalytically inactive LPP3 mutant reduces the formation of Rab6 transport carriers and the retrograde protein transport

Our next step was to test whether the expression of the wild-type (LPP3wt) and the catalytically inactive mutant (LPP3S197T; Escalante-Alcalde et. al., 2003) forms of human LPP3 affected protein transport at the ER/Golgi interface. First, we examined the formation of Rab6-containing transport carriers. When LPP3wt and Rab6 were co-expressed, both proteins colocalized at the Golgi and in cytoplasmic vesicular structures (Fig. 6A; see arrowheads in magnified boxes). The presence of both proteins in

transport carriers provides no information about their directionality, since Rab6-containing transport carriers transit anterogradely to the plasma membrane (Grigoriev et. al., 2007 and 2011) and retrogradely to the ER (White et al., 1999). To investigate whether some of these vesicular structures mediate in retrograde transport, we examined the colocalization of LPP3wt-GFP with internalized cy3-STxB. After 2 h of STxB internalization at 37ºC followed by 1 h at 15ºC, colocalization of LPP3 with STxB was seen in some vesicular structures (Fig 6B and magnified boxes). Rab6 and LPP3 colocalization at the Golgi and in vesicular structures was seen only in cells expressing moderate levels of Rab6-myc. Conversely, cells expressing high levels of Rab6-myc either alone or together with LPP3-GFP showed a complete redistribution of Rab6 into the ER (supplementary Fig. 8). This observation is in accordance with the previously reported BFA-like phenotypical effect caused by Rab6wt or GTP-bound overexpression (Martínez et. al., 1997). Remarkably, the co-expression of Rab6-myc with the catalytically inactive LPP3 mutant (LPP3S193T-GFP) strongly reduced the redistribution of Rab6wt to the ER, with the concomitant increase of Rab6 still present in the Golgi (supplementary Fig. 8A and B).

To study whether this blockade in the Rab6 redistribution to the ER caused by LPP3S197T mutant was due to inhibition of Golgi-to-ER retrograde transport, we monitored the arrival of retrograde cargo at the ER. In this case, we measured the colocalization of STxB with LPP3wt-GFP or LPP3S197T-GFP at the ER in COS-7 cells after 2 h of internalization of STxB at 37ºC, followed by 1 h at 15ºC and an additional hour of rewarming. At this time, in cells expressing LPP3wt part of STxB had reached the nuclear envelope, which was not the case in cells expressing the LPP3S197T mutant form (Fig. 6C and D).

Collectively, these results indicate that LPP3wt-GFP associates with Rab6 transport carriers, which are in part transported from the Golgi to the ER, and that the expression of the catalytically inactive mutant and the silencing of LPP3 produce similar defects in Rab6-dependent retrograde protein transport.

Ultrastructural alterations in the ER/Golgi interface in LPP3-silenced cells

We examined the ultrastructure in the ER/Golgi interface area in Swiss 3T3 cells depleted of LPP3 by means of the lentiviral shRNA system. Unlike control cells (Fig. 7A), LPP3-silenced cells showed some slightly swollen cisternae (Fig. 7C) and an invariably abnormal accumulation of numerous vesicular membrane profiles as well as

membrane buds attached to Golgi cisternae and peri-Golgi tubulovesicular structures (dotted circles in Fig. 7B and Fig. 7D). Interestingly, some budding profiles clearly contained an electrondense material attached to the cytoplasmic face, which indicates the presence of the coatomer (Fig. 7D, red arrows) while others did not show this electrondense content. No alterations in the ER were observed. Together, data supports the participation of LPP3 in the formation of COPI-dependent and COPI-independent transport carriers at the ERGIC and Golgi.

Alterations in the homeostasis of DAG in LPP3-silenced cells

To assess whether the aforementioned alterations in the ER/Golgi interface protein transport in LPP3-silenced cells were caused by changes in the phosphatidic acid (PA)-derived DAG, we first measured the production of DAG, triacylglycerol (TAG) and major phospholipids using radioactive labeling. The [^{14}C]acetate incorporation into DAG, TAG, and major phospholipids decreased in LPP3-silenced cells (Figs. 8A and C), which indicates that the newly synthetized DAG is reduced, which compromises the *de novo* synthesis of TAG and phospholipids in LPP3- silenced cells. Consistent with this conclusion, the incorporation of [^{14}C]acetate into PA as a percentage of total [^{14}C]acetate incorporation into the lipids was higher in LPP3-silenced cells than in control cells (Fig. 8B), indicating the accumulation of the *de novo* synthesized PA. To investigate whether the reduction of newly synthesized phospholipids was compensated by an enhancement of the recycling pathways, we examined the incorporation of [^{32}P]orthophosphoric acid. We observed that the [^{32}P]-labeling of major phospholipids was similar in control and LPP3-silenced cells (Fig. 8D), which confirmed a higher recycling of phospholipids in LPP3-silenced cells, compared to controls.

Next, we examined whether the DAG pool present in Golgi membranes was also affected after the silencing of LPP3. To this end, we expressed the GFP-tagged C1b domain of PKCθ (GFP-C1b), which in control conditions localizes to the Golgi and acts as a dynamic sensor of DAG content in this compartment (Carrasco and Merida, 2004; Fernandez-Ulibarri et al., 2007). LPP3-silenced Swiss 3T3 cells showed lesser GFP-C1b domain in the Golgi than control cells (Suppl. Fig. 9). Taken together, these results indicate that the depletion of LPP3 reduced *de novo* synthesized DAG and the Golgi-associated DAG content.

DISCUSSION

Here we provide evidence that human LPP3 is present in compartments of the secretory pathway from ERES to the *trans*-Golgi. The localization of LPP3 in the ER and the ERGIC is consistent with the presence of different pools of LPP3, one non-glycosylated and with immature N-glycans (Endo-H sensitive), and the other with mature N-glycans (Endo-H resistant) (Sciorra and Morris, 1999). Remarkably, the time-lapse analysis of LPP3 transport at the ER/Golgi interphase strongly suggests that part of the protein constitutively cycles between the ER and the Golgi, and behaves like an ERGIC-resident protein. The association of the overexpressed LPP3 with the STxB in vesicular structures directed to the ER indicates that LPP3 retrograde transport from the Golgi is partly Rab6-dependent. We also notice that unlike LPP1 and LPP2 isoforms, LPP3 contains the sequence KTKTT in the position 279-283 of its cytoplasmic C-terminus, which matches one of the two canonical motifs (KXKXX and KKXX) by which integral membrane proteins are incorporated into COPI transport carriers (Beck et al., 2009; Jackson et al., 1990; Nilsson et al., 1989). This could explain the interaction of LPP3 with the COPI machinery, which is later retrieved from the ERGIC and Golgi membranes and carried back to the ER and ERGIC respectively, in a similar manner to other ERGIC proteins such as ERGIC53, KDELr, and Sac1 (Cabrera et al., 2003; Rohde et al., 2003; Schindler et al., 1993). Whatever the mechanism by which LPP3 recycles at the ER/Golgi interface, some of it escapes from the retrieval system to complete N-glycosylation at distal Golgi membranes and it finally reaches the plasma membrane, where it seems to associate with lipid rafts (Kai et al., 2006).

LPP3 metabolizes lipids involved in early secretory membrane trafficking

The enzymatic machinery that regulates membrane lipids in compartments of the secretory pathway determines their morphology, associated membrane trafficking and lipid-protein interaction (Bechler et al., 2010; Ben-Tekaya et al., 2010; Brown et al., 2003; de Figueiredo et al., 2000; Morikawa et al., 2009; San Pietro et al., 2009; Schmidt and Brown, 2009; Subathra et al., 2011). Here we incorporate LPP3 into the enzymatic machinery (PLD, SMS, LPAAT3, and PLA_2) already related to the generation of the DAG necessary for the transport carrier formation along the secretory pathway. The observation that the depletion of LPP3 reduces [^{14}C]acetate incorporation into DAG and TAG, as well as into the major phospholipid classes, points to inhibition of the *de novo* synthesis of glycerolipids in LPP3-silenced cells. Taking into account that the

conversion of PA to DAG is a necessary step for the *de novo* synthesis of phospatidylcholine (PC), phosphatidylethanolamide (PE) and phosphatidylserine (PS), as well as the neutral lipid TAG, we postulate that LPP3 generates DAG by dephosphorylating the *de novo* synthesized PA in addition to the PA that comes from the PLD-induced hydrolysis of PC (Sciorra and Morris, 1999). The increase in [^{14}C]acetate labeled PA supports this idea. On the other hand, the observation that the labeling of major phospholipids with [^{32}P]orthophosphoric acid (PC, SM, PE, PS, and PI) is the same in control and LPP3-silenced cells indicates that the recycling pathways for the synthesis of phospholipids maintain the same levels of phospholipids in LPP3-silenced cells as those in control cells. Besides, we observed a reduction in Golgi-associated DAG.

LPP3 in the transport carrier formation process and in protein transport at the ER/Golgi interface

Here we show that propanolol and LPP3 depletion cause similar impairments in the formation of ERGIC tubules. We consider that DAG formation mediated by LPP3 is required for the budding of highly curved tubular transport carriers from the ERGIC (and Golgi) membranes, since the addition of DOG (a short chain cell membrane-permeant DAG) prevented the inhibitory effects caused by the depletion of LPP3. In this context, recent studies have suggested a role for PA-derived DAG in the budding stage of transport carrier formation in Golgi membranes (Asp et al., 2009). This work showed that in the presence of 300 µM propanolol, which completely inhibits the PAP1 and PAP2 families of enzymes, Golgi cisternae remain flat without any omega profiles (which is indicative of vesicle formation), suggesting that PAP1 and PAP2 were involved in the initial budding stage. However, we reported earlier that 60 µM propanolol, which does not completely inhibit PAP1 proteins (Meier et al., 1998) and does not perturb the microtubular network, induced the accumulation of COPI-coated budding vesicles at the Golgi and peri-Golgi membranes (Fernandez-Ulibarri et al., 2007), thus implicating PAP2 enzymes in the fission step of vesicle generation. Thus, these previous results and those reported here indicate that PAP1 and the PAP2 subtype LPP3 could cooperate in the formation of transport carriers both in the ERGIC and in the Golgi. Likewise, LPP3 seems to regulate budding and fission at the Golgi, since the decrease in the number of Rab6-GFP transport carriers occurring when the PAP activity was inhibited by propanolol, LPP3 was silenced or the catalytically inactive LPP3 was

expressed indicates that budding is impaired. The concomitant increase in the length of the Rab6 tubules also points to a defect in the final fission of these tubules. Therefore, we envision a model in which, at an early stage, LPP3 (whose catalytic domain faces the lumen) would form DAG (a cone-shape lipid) in the inner leaflet of the bilayer. At this stage LPP3 could coordinately act with $cPLA_2$, which forms LPA (an inverted cone-shape lipid, which in turn might be enhanced by the inhibition of LPP3) in the cytoplasmic leaflet of the bilayer (de Figueiredo et al., 2000; San Pietro et al., 2009; Yang et al., 2011), allowing membranes to bend outward into the cytosol, thereby facilitating initial budding. Although there are no experimental data showing the precise localization of DAG in a budding vesicle/tubule, the strong negative curvatures generated in the neck clearly require DAG and its spontaneous flip-flop between the two membrane leaflets. On the other hand, the presence of DAG permits and enhances the negative curvature necessary for the recruitment of ArfGAP1 through its ALP motif (Antony et al., 1997; Ambroggio et al., 2010). Thus, local DAG accumulation and the increased recruitment of ARFGAP1 could act together, leading to the progressive pre-fission constriction of the neck in such a way that final vesicle/tubule scission could occur even without the involvement of a fission protein. In any case, whatever the biophysical mechanism involved or the stage in the transport carrier formation in which LPP3 participates, cargo trafficking at the ER/Golgi interface should be affected. This is indeed the case in LPP3-silenced cells and in cells overexpressing a catalytically inactive form of LPP3, where retrograde cargo (STxB) transport is impaired. Although the transport of VSV-G from the ER to the Golgi was unaltered in LPP3-silenced cells, we observed increased colocalization of ERGIC53-GFP with ssDsRed after the rewarming to 37°C from 15°C. A possible explanation for this apparent discrepancy is that the depletion of LPP3 perturbs the maturation and/or sorting functions of ERGIC compartment. In contraposition to the maturation model, in which ERGIC clusters would represent transport vehicles for protein delivery to the Golgi, recent studies show that the ERGIC is a stable compartment which is made-up of numerous discontinuous elements that function in bidirectional sorting to the ER and to the Golgi. The reduction in the number of ERGIC53-GFP elements (with the concomitant increase in their size) as well as the greater association of ERGIC53-GFP with the ssDsRed secretory protein seen in LPP3-silenced cells indicates that ERGIC-resident proteins (such as ERGIC53) cannot be efficiently sorted from transport carriers that contain anterograde protein cargo (such as ssDsRed). Then, tubulation could be more involved in the

interconnection and membrane exchange occurring between ERGIC stationary clusters (which would determine the steady number of ERGIC dot-like structures at physiological conditions) rather than a critical process for transport of anterograde cargo at the ER-Golgi interphase. Likewise, the decrease in density of ERGIC clusters could result from impairment in the retrograde transport from the *cis*-Golgi to the ERGIC, which is supported by the delay in the STxB-KDEL transport from the Golgi to the ER and the accumulation of uncompleted fissioned buds in Golgi cisternae.

Remarkably, the retrograde trafficking impairment occurring in LPP3-depleted cells does not distinguish between COPI-dependent and COPI-independent mechanisms, as both wild type STxB (COPI-independent) and STxB-KDEL (COPI-dependent) were equally perturbed in LPP3-silenced cells. These results suggest that the DAG pool derived from the LPP3 activity is involved more in generating the membrane curvature than in acting as an acceptor for the recruitment of a specific molecular machinery that discriminates between the COPI-dependent or COPI-independent retrograde protein transports.

In conclusion, our study shows that LPP3, *en route* to the plasma membrane (where it has a variety of physiological functions (for details see Escalante-Alcalde et. al., 2003; Long et. al., 2005; Humtsoe et. al., 2010), acts in early compartments of the secretory pathway, in particular in the formation of retrograde transport carriers. LPP3 dephosphorylates at least *de novo* synthesized PA to generate DAG, which is in turn necessary for the aforementioned transport process. Thus, LPP3 can be added to the increasing arsenal of enzymatic machinery that regulates the lipid metabolism of secretory compartments, which contributes to the formation of transport carriers.

MATERIAL AND METHODS

Please see online Supplementary data for the expanded Material and Methods section.

LPP3 silencing and plasmids transfection

The negative control non-targeting pool of siRNAs and the siRNA sequences against human LPP3 - oligonucleotide #6 (5'-GGGACUGUCUCGCGUAUCA-3') and oligonucleotide #8 (5'-GGACAUUAUUGACAGGAAC-3') were obtained from Dharmacon (Lafayette, CO, USA). SiRNA transfections were performed using Hiperfect (Hilden, Germany) according to the manufacturer's instructions. Briefly, HeLa cells were seeded at a density of 10^5 cells in 6-well culture plates for 24 h. Thereafter, cells were transfected for 48 h with the indicated oligonucleotides alone or both together at a final concentration of 20 nM when added individually or 10 nM for each oligo when added together. Subsequently, cells were detached with trypsin, re-seeded at a density of 4 x 10^5 cells/well in 6-well culture plates and subjected to a second round of reverse transfection for 24 h more. Therefore, silencing experiments were carried out for a total of 72 h, after which time cells were collected for Western blot or fixed for immunofluorescence analysis. Control cells were mock transfected or, where indicated, transfected with the non-targeting pool of siRNAs following the protocol described above.

For rescue experiments cells were transfected with the murine form of LPP3 24 h before the total 72 h of siRNA human LPP3 transfection.

For LPP3 silencing using lentiviral-based system in Swiss 3T3, the hairpin sequences designed against mouse LPP3 mRNA were the following: TRC49/TRCN0000081249 (5'CCGGCGGGTATCTGACTACAAGCATCTCGAGATTTGTAGTCACCGTTG3') and TRC51/TRCN0000081251 (5'CCGGCCTGATTTCAGTCAGATCAATCTCGAG AGATCTGACCTGTTTTTG3') and they were purchased from Open Biosystems (Huntsville, AL, USA). Clone details for creating shRNAs against LPP3 are available online (http://openbiosystems.com). The viral particles were produced by transient co-transfection of plasmid encoding LPP3 shRNA and packaging vectors into 293T cells using Lipofectamine 2000 (Invitrogen, Paisley, United Kingdom). The resulting supernatant was collected after 96 h. For the infection, Swiss 3T3 cells were seeded at a density of 6 x 10^5 cells in 100 cm^2 plates for 24 h. Thereafter, lentiviral particles

containing shRNAs were added to the culture medium for 24 h. The post-transduction culture medium was subsequently replaced with complete DMEM supplemented with puromycin (3µg/ml). After 96 h, infected cells were collected for Western blotting or fixed for immunofluorescence analysis. Control Swiss 3T3 cells were infected with lentiviral particles lacking the plasmids containing the LPP3 shRNAs. For plasmid transfections, Fugene (Promega) were used for HeLa cells and Lipofectamine 2000 for Swiss3T3 and 293T cells, following the manufacturer's instructions in all cases.

Inmunofluorescence

Indirect immunofluorescence assays were carried out as previously described (Fernández-Ulibarri et al., 2007), except when the tubulation of the ERGIC was examined. In this case, cells were first fixed at 37°C with 4% paraformaldehyde (PFA) in PBS for 10 min followed by additional 10 min of fixation at room temperature. The antibodies were used at the following dilutions: anti-LPP3 (1:100), anti-KDELr (1:500), anti-Golgin97 (1:500), anti-GM130 (1:1000), anti-EEA1 (1:50), anti-mouse-Cy3 (1:200), anti-mouse-Alexa488 (1:100), anti-rabbit-Cy3 (1:200) and anti-rabbit-Alexa488 (1:100). Coverslips were mounted on microscope slides using Mowiol (Calbiochem). Microscopy and imaging were performed either with an Olympus BX60 epifluorescence microscope equipped with a cooled Olympus CCD camera (Lake Success, NY) or with a TCS-SL laser scanning confocal spectral microscope (Leica Microsystems, Mannheim, Germany). Confocal images were taken with a PL APO x63 (NA 1.32) or PL APO x100 (NA 1.4) objectives. For each cell, different images with an optical size of 0.5 µm from the ventral surface to the top of the cell were acquired.

Live Imaging

Time-lapse fluorescence confocal microscopy experiments were carried out using a TCS-SL laser-scanning confocal spectral microscope (see above) equipped with an incubation system with temperature and CO_2 control. GFP images were acquired with an PL APO 100x (NA 1,4) objective, 488-nm laser line (excitation intensity 15%), excitation beam splitter RSP 500, emission range detection: 500–610 nm and the confocal pinhole set at 1 Airy unit. Images were recorded at 0.6 s intervals for a maximum of 15 min and processed using the freeware ImageJ. Filters were used to optimize each experiment. For the analysis of ERGIC53-GFP and Rab6-GFP tubulation, the initial frame was acquired immediately after shifting cells from a temperature-controlled incubator at 15°C to another incubation system coupled to the

TCS-SL confocal at 37°C. In the experiments with ERGIC53-GFP, where indicated, propanolol was added 5 min before the shift from 15°C to 37°C. In the reversion experiment, propranolol containing media was carefully replaced after 6 min of incubation of cells at 37°C by adding fresh media. In the experiments with Rab6-GFP, propanolol was added at the moment of the temperature shift.

Transmission electron microscopy.

For transmission electron microscopy (TEM), Swiss 3T3 cells infected with the LPP3 shRNAlentivirus were rapidly fixed after 96 h post-infection with 1.25% glutaraldehyde in PIPES buffer (0.1 M, pH 7.4) containing sucrose (2%) and Mg_2SO_4 (2 mM) for 60 min at 37 °C. Cells were then gently scraped, pelleted at 100 x *g* for 10 min, rinsed in PIPES buffer (3 x 5 min), and postfixed with 1% (wt/vol) OsO_4, 1% (wt/vol) $K_3Fe(CN)_6$ in PIPES buffer for 1 h at room temperature in the dark. They were then treated for 5 min with tannic acid (0.1%) in PIPES buffer, rinsed in distilled water, block-stained with 1% uranyl acetate in 70% ethanol for 1 h, dehydrated with graded ethanol solutions, and finally embedded in Epon plastic resin (EMS, Hatfield, PA). Ultrathin sections were stained with lead citrate and observed on a JEOL 1010 electron microscope (Peabody, MA). Micrographs of randomly selected areas were obtained with a GatanBioscan digital camera (Pleasanton, CA) at the same final magnification.

Determination of lipid labeling

Control and silenced cells were labeled with 5 μCi/ml [^{32}P]orthophosphoric acid or 1 μCi/ml [^{14}C]acetate for the last 24 h of LPP3 silencing. Lipids were extracted as previously described (Sarri et al., 2011). Individual lipid classes were separated by TLC, identified with authentic standards, and counted for radioactivity. Major phospholipid classes such as phosphatidylethanolamine (PE), phosphatidylcholine (PC), sphingomyelin (SM), phosphoinositol (PI) and phosphatidylserine (PS), as well as phosphatidic acid (PA) in [^{14}C]- and [^{32}P]-labeled lipid extracts were separated in two-dimensional thin layer chromatography (TLC) with the following mobile phases: first, chloroform/methanol/NH_4OH (65:35:10 by volume); second, chloroform/methanol/acetone/acetic acid/water (10:2:4:2:1 by volume). Neutral lipids such as triacylglycerol (TAG) and diacylglycerol (DAG) in [^{14}C]-acetate-labeled lipid extracts were separated by two-dimensional TLC with the mobile phases: first: chloroform/methanol (10:1 v/v); second: hexane/diethyl ether/acetic acid (70:30:1 by

volume). The [^{14}C]-labeled lipids and the [^{32}P]-labeled phospholipids separated in the TLC plates were counted for radioactivity with a PhosphorImager (Typhon TRIO, Amersham Biosciences), and analyzed with ImageQuant software (Amersham Biosciences).

Acknowledgements. We thank our colleagues for generously providing antibodies, plasmids and cells used in this study, Maite Muñoz for technical support, staff of SCT-UB for confocal microscope advice, Rosa M. Rios for helping us in the production of lentiviral particles containing shRNAs against LPP3, Jean-Baptiste Manneville and members of the lab for helpful discussions, and Robin Rycroft for editorial assistance. This study was financed with a grant (BFU2009-07186) to G.E. E.G-M. is a predoctoral fellow from AGAUR (Generalitat de Catalunya, Catalunya, Spain). G.E. dedicates this article to his late father Victoriano Egea-López and to his uncle Joaquín Egea-López.

REFERENCES

Alderton, F., Darroch, P., Sambi, B., McKie, A., Ahmed, I. S., Pyne, N. and Pyne, S. (2001). G-protein-coupled receptor stimulation of the p42/p44 mitogen-activated protein kinase pathway is attenuated by lipid phosphate phosphatases 1, 1a, and 2 in human embryonic kidney 293 cells. *J. Biol. Chem.* **276**, 13452-13460.

Ambroggio, E., Sorre, B., Bassereau, P., Goud, B., Manneville, J. B. and Antonny, B. (2010). ArfGAP1 generates an Arf1 gradient on continuous lipid membranes displaying flat and curved regions. *EMBO J.* **29**, 292-303.

Antony,B., Huber,I., Paris,S., Chabre,M., and Cassel,D. (1997). Activation of ADP-ribosylation factor 1 GTPase-activating protein by phsphatidylcholine-derived diacylglycerols. J. Biol. Chem. **272**, 30848-30851.

Asp, L., Kartberg, F., Fernandez-Rodriguez, J., Smedh, M., Elsner, M., Laporte, F., Barcena, M., Jansen, K. A., Valentijn, J. A., Koster, A. J. et al. (2009). Early stages of Golgi vesicle and tubule formation require diacylglycerol. *Mol. Biol. Cell* **20**, 780-790.

Bard, F. and Malhotra, V. (2006). The formation of TGN-to-plasma-membrane transport carriers. *Annu. Rev. Cell Dev. Biol.* **22**, 439-455.

Baron, C. L. and Malhotra, V. (2002). Role of diacylglycerol in PKD recruitment to the TGN and protein transport to the plasma membrane. *Science* **295**, 325-328.

Bechler, M. E., Doody, A. M., Racoosin, E., Lin, L., Lee, K. H. and Brown, W. J. (2010). The phospholipase complex PAFAH Ib regulates the functional organization of the Golgi complex. *J. Cell Biol.* **190**, 45-53.

Beck, R., Rawet, M., Wieland, F. T. and Cassel, D. (2009). The COPI system: molecular mechanisms and function. *FEBS Lett.* **583**, 2701-2709.

Ben-Tekaya, H., Kahn, R. A. and Hauri, H. P. (2010). ADP ribosylation factors 1 and 4 and group VIA phospholipase A regulate morphology and intraorganellar traffic in the endoplasmic reticulum-Golgi intermediate compartment. *Mol. Biol. Cell* **21**, 4130-4140.

Ben-Tekaya, H., Miura, K., Pepperkok, R. and Hauri, H. P. (2005). Live imaging of bidirectional traffic from the ERGIC. *J. Cell Sci.* **118**, 357-367.

Billah, M. M., Eckel, S., Mullmann, T. J., Egan, R. W. and Siegel, M. I. (1989). Phosphatidylcholine hydrolysis by phospholipase D determines phosphatidate and diglyceride levels in chemotactic peptide-stimulated human neutrophils. Involvement of phosphatidate phosphohydrolase in signal transduction. *J. Biol. Chem.* **264**, 17069-17077.

Brindley, D. N. and Pilquil, C. (2009). Lipid phosphate phosphatases and signaling. *J. Lipid Res.* **50** Suppl, S225-S230.

Brindley, D. N., Pilquil, C., Sariahmetoglu, M. and Reue, K. (2009). Phosphatidate degradation: phosphatidate phosphatases (lipins) and lipid phosphate phosphatases. *Biochim. Biophys. Acta* **1791**, 956-961.

Brown, W. J., Chambers, K. and Doody, A. (2003). Phospholipase A2 (PLA2) enzymes in membrane trafficking: mediators of membrane shape and function. *Traffic.* **4**, 214-221.

Burger, K. N. (2000). Greasing membrane fusion and fission machineries. *Traffic.* **1**, 605-613.

Cabrera, M., Muniz, M., Hidalgo, J., Vega, L., Martin, M. E. and Velasco, A. (2003). The retrieval function of the KDEL receptor requires PKA phosphorylation of its C-terminus. *Mol. Biol. Cell* **14**, 4114-4125.

Carrasco, S. and Merida, I. (2004). Diacylglycerol-dependent binding recruits PKCtheta and RasGRP1 C1 domains to specific subcellular localizations in living T lymphocytes. *Mol. Biol. Cell* **15**, 2932-2942.

de Figueiredo, P., Drecktrah, D., Polizotto, R. S., Cole, N. B., Lippincott-Schwartz, J. and Brown, W. J. (2000). Phospholipase A2 antagonists inhibit constitutive retrograde membrane traffic to the endoplasmic reticulum. *Traffic.* **1**, 504-511.

Dejgaard, S. Y., Murshid, A., Dee, K. M. and Presley, J. F. (2007). Confocal microscopy-based linescan methodologies for intra-Golgi localization of proteins. *J. Histochem. Cytochem.* **55**, 709-719.

Escalante-Alcalde, D., Hernandez, L., Le, S. H., Maeda, R., Lee, H. S., Jr, G. C., Sciorra, V. A., Daar, I., Spiegel, S., Morris, A. J. et al. (2003). The lipid phosphatase LPP3 regulates extra-embryonic vasculogenesis and axis patterning. *Development* **130**, 4623-4637.

Fernandez-Ulibarri, I., Vilella, M., Lazaro-Dieguez, F., Sarri, E., Martinez, S. E., Jimenez, N., Claro, E., Merida, I., Burger, K. N. and Egea, G. (2007). Diacylglycerol is required for the formation of COPI vesicles in the Golgi-to-ER transport pathway. *Mol. Biol. Cell* **18**, 3250-3263.

Grigoriev, I., Splinter, D., Keijzer, N., Wulf, P. S., Demmers, J., Ohtsuka, T., Modesti, M., Maly, I. V., Grosveld, F., Hoogenraad, C. C. et al. (2007). Rab6 regulates transport and targeting of exocytotic carriers. *Dev. Cell* **13**, 305-314.

Grigoriev, I., Yu, K. L., Martinez-Sanchez, E., Serra-Marques, A., Smal, I., Meijering, E., Demmers, J., Peränen, J., Pasterkamp, R. J., van der Sluijs, P. et al. (2011). Rab6, Rab8, and MICAL3 cooperate in controlling docking and fusion of exocytotic carriers. *Curr. Biol.* **21**, 967-974.

Grimsey, N., Han, G. S., O'Hara, L., Rochford, J. J., Carman, G. M. and Siniossoglou, S. (2008). Temporal and spatial regulation of the phosphatidate phosphatases lipin 1 and 2. *J. Biol. Chem.* **283**, 29166-29174.

Hammond, A. T. and Glick, B. S. (2000). Dynamics of transitional endoplasmic reticulum sites in vertebrate cells. *Mol. Biol. Cell* **11,** 3013-3030.

Henneberry, A. L., Wright, M. M. and McMaster, C. R. (2002). The major sites of cellular phospholipid synthesis and molecular determinants of Fatty Acid and lipid head group specificity. *Mol. Biol. Cell* **13**, 3148-3161.

Ho, W. C., Allan, V. J., van Meer G., Berger, E. G. and Kreis, T. E. (1989). Reclustering of scattered Golgi elements occurs along microtubules. *Eur. J. Cell Biol.* **48**, 250-263.

Huijbregts, R. P., Topalof, L. and Bankaitis, V. A. (2000). Lipid metabolism and regulation of membrane trafficking. *Traffic.* **1**, 195-202.

Humtsoe, J. O., Liu, M., Malik, A. B. and Wary, K. K. (2010). Lipid phosphate phosphatase 3 stabilization of beta-catenin induces endothelial cell migration and formation of branching point structures. *Mol. Cell. Biol.* **30**, 1593-1606.

Jackson, M. R., Nilsson, T. and Peterson, P. A. (1993). Retrieval of transmembrane proteins to the endoplasmic reticulum. *J. Cell Biol.* **121**, 317-333.

Jasinska, R., Zhang, Q. X., Pilquil, C., Singh, I., Xu, J., Dewald, J., Dillon, D. A., Berthiaume, L. G., Carman, G. M., Waggoner, D. W. et al. (1999). Lipid phosphate phosphohydrolase-1 degrades exogenous glycerolipid and sphingolipid phosphate esters. *Biochem. J.* **340** (Pt 3), 677-686.

Johannes, L., Tenza, D., Antony, C. and Goud, B. (1997). Retrograde transport of KDEL-bearing B-fragment of Shiga toxin. *J. Biol. Chem.* **272**, 19554-19561.

Kano, F., Tanaka, A. R., Yamauchi, S., Kondo, H. and Murata, M. (2004). Cdc2 kinase-dependent disassembly of endoplasmic reticulum (ER) exit sites inhibits ER-to-Golgi vesicular transport during mitosis. *Mol. Biol. Cell* **15**, 4289-4298.

Kai, M., Sakane, F., Jia, Y. J., Imai, S., Yasuda, S. and Kanoh, H. (2006). Lipid phosphate phosphatases 1 and 3 are localized in distinct lipid rafts. *J. Biochem.* **140**, 677-686.

Kai, M., Wada, I., Imai, S., Sakane, F. and Kanoh, H. (1997). Cloning and characterization of two human isozymes of Mg2+-independent phosphatidic acid phosphatase. *J. Biol. Chem.* **272**, 24572-24578.

Kearns, B. G., McGee, T. P., Mayinger, P., Gedvilaite, A., Phillips, S. E., Kagiwada, S. and Bankaitis, V. A. (1997). Essential role for diacylglycerol in protein transport from the yeast Golgi complex. *Nature* **387**, 101-105.

Klumperman, J., Schweizer, A., Clausen, H., Tang, B. L., Hong, W., Oorschot, V. and Hauri, H. P. (1998). The recycling pathway of protein ERGIC-53 and dynamics of the ER-Golgi intermediate compartment. *J. Cell Sci.* **111**, 3411-3425.

Kooijman, E. E., Chupin, V., Fuller, N. L., Kozlov, M. M., de, K. B., Burger, K. N. and Rand, P. R. (2005). Spontaneous curvature of phosphatidic acid and lysophosphatidic acid. *Biochemistry* **44**, 2097-2102.

Krauss, M., Jia, J. Y., Roux, A., Beck, R., Wieland, F. T., De, C. P. and Haucke, V. (2008). Arf1-GTP-induced tubule formation suggests a function of Arf family proteins in curvature acquisition at sites of vesicle budding. *J. Biol. Chem.* **283**, 27717-27723.

Lev, S. (2006). Lipid homoeostasis and Golgi secretory function. *Biochem. Soc. Trans.* **34**, 363-366.

Lippincott-Schwartz, J. and Phair, R. D. (2010). Lipids and cholesterol as regulators of traffic in the endomembrane system. *Annu. Rev. Biophys.* **39**, 559-578.

Litvak, V., Dahan, N., Ramachandran, S., Sabanay, H. and Lev, S. (2005). Maintenance of the diacylglycerol level in the Golgi apparatus by the Nir2 protein is critical for Golgi secretory function. *Nat. Cell Biol.* **7**, 225-234.

Long, J., Darroch, P., Wan, K. F., Kong, K. C., Ktistakis, N., Pyne, N. J. and Pyne, S. (2005). Regulation of cell survival by lipid phosphate phosphatases involves the modulation of intracellular phosphatidic acid and sphingosine 1-phosphate pools. *Biochem. J.* **391**, 25-32.

Long, J. S., Pyne, N. J. and Pyne, S. (2008). Lipid phosphate phosphatases form homo- and hetero-oligomers: catalytic competency, subcellular distribution and function. *Biochem. J.* **411**, 371-377.

Martinez, O., Antony, C., Pehau-Arnaudet, G., Berger, E.G., Salamero, J. and Goud, B. (1997). GTP-bound forms of rab6 induce the redistribution of Golgi proteins into the endoplasmic reticulum. *Proc. Natl. Acad. Sci. U. S. A* **94**, 1828-1833.

Martinez-Alonso, E., Ballesta, J. and Martinez-Menarguez, J. A. (2007). Low-temperature-induced Golgi tubules are transient membranes enriched in molecules regulating intra-Golgi transport. *Traffic.* **8**, 359-368.

Meier, K. E., Gause, K. C., Wisehart-Johnson, A. E., Gore, A. C., Finley, E. L., Jones, L. G., Bradshaw, C. D., McNair, A. F. and Ella, K. M. (1998). Effects of propranolol on phosphatidate phosphohydrolase and mitogen-activated protein kinase activities in A7r5 vascular smooth muscle cells. *Cell Signal.* **10**, 415-426.

Merida, I., Avila-Flores, A. and Merino, E. (2008). Diacylglycerol kinases: at the hub of cell signalling. *Biochem. J.* **409**, 1-18.

Morikawa, R. K., Aoki, J., Kano, F., Murata, M., Yamamoto, A., Tsujimoto, M. and Arai, H. (2009). Intracellular phospholipase A1gamma (iPLA1gamma) is a novel factor involved in coat protein complex I- and Rab6-independent retrograde transport between the endoplasmic reticulum and the Golgi complex. *J. Biol. Chem.* **284**, 26620-26630.

Morris, K. E., Schang, L. M. and Brindley, D. N. (2006). Lipid phosphate phosphatase-2 activity regulates S-phase entry of the cell cycle in Rat2 fibroblasts. *J. Biol. Chem.* **281**, 9297-9306.

Nagaya, H., Wada, I., Jia, Y. J. and Kanoh, H. (2002). Diacylglycerol kinase delta suppresses ER-to-Golgi traffic via its SAM and PH domains. *Mol. Biol. Cell* **13**, 302-316.

Nilsson, T., Jackson, M. and Peterson, P. A. (1989). Short cytoplasmic sequences serve as retention signals for transmembrane proteins in the endoplasmic reticulum. *Cell* **58**, 707-718.

Pappu, A. S. and Hauser, G. (1983). Propranolol-induced inhibition of rat brain cytoplasmic phosphatidate phosphohydrolase. *Neurochem. Res.* **8**, 1565-1575.

Pyne, S., Lee, S. C., Long, J. and Pyne, N. J. (2009). Role of sphingosine kinases and lipid phosphate phosphatases in regulating spatial sphingosine 1-phosphate signalling in health and disease. *Cell Signal.* **21**, 14-21.

Pyne, S., Long, J. S., Ktistakis, N. T. and Pyne, N. J. (2005). Lipid phosphate phosphatases and lipid phosphate signalling. *Biochem. Soc. Trans.* **33**, 1370-1374.

Roberts, R., Sciorra, V. A. and Morris, A. J. (1998). Human type 2 phosphatidic acid phosphohydrolases. Substrate specificity of the type 2a, 2b, and 2c enzymes and cell surface activity of the 2a isoform. *J. Biol. Chem.* **273**, 22059-22067.

Rohde, H. M., Cheong, F. Y., Konrad, G., Paiha, K., Mayinger, P. and Boehmelt, G. (2003). The human phosphatidylinositol phosphatase SAC1 interacts with the coatomer I complex. *J. Biol. Chem.* **278**, 52689-52699.

Roth, M. G. (2008). Molecular mechanisms of PLD function in membrane traffic. *Traffic.* **9**, 1233-1239.

Roux, A., Cuvelier, D., Nassoy, P., Prost, J., Bassereau, P. and Goud, B. (2005). Role of curvature and phase transition in lipid sorting and fission of membrane tubules. *EMBO J.* **24**, 1537-1545.

San Pietro, E., Capestrano, M., Polishchuk, E. V., DiPentima, A., Trucco, A., Zizza, P., Mariggio, S., Pulvirenti, T., Sallese, M., Tete, S. et al. (2009). Group IV phospholipase A(2)alpha controls the formation of inter-cisternal continuities involved in intra-Golgi transport. *PLoS. Biol.* **7**, e1000194.

Saraste, J. and Svensson, K. (1991). Distribution of the intermediate elements operating in ER to Golgi transport. *J. Cell Sci.* **100**, 415-430.

Sarri, E., Sicart, A., Lazaro-Dieguez, F. and Egea, G. (2011). Phospholipid synthesis participates in the regulation of diacylglycerol required for membrane trafficking at the Golgi complex. *J. Biol. Chem.* **286**, 28632-28643.

Schindler, R., Itin, C., Zerial, M., Lottspeich, F. and Hauri, H. P. (1993). ERGIC-53, a membrane protein of the ER-Golgi intermediate compartment, carries an ER retention motif. *Eur. J. Cell Biol.* **61**, 1-9.

Schmidt, J. A. and Brown, W. J. (2009). Lysophosphatidic acid acyltransferase 3 regulates Golgi complex structure and function. *J. Cell Biol.* **186**, 211-218.

Sciorra, V. A. and Morris, A. J. (1999). Sequential actions of phospholipase D and phosphatidic acid phosphohydrolase 2b generate diglyceride in mammalian cells. *Mol. Biol. Cell* **10**, 3863-3876.

Shemesh, T., Luini, A., Malhotra, V., Burger, K. N. and Kozlov, M. M. (2003). Prefission constriction of Golgi tubular carriers driven by local lipid metabolism: a theoretical model. *Biophys. J.* **85**, 3813-3827.

Sigal, Y. J., McDermott, M. I. and Morris, A. J. (2005). Integral membrane lipid phosphatases/phosphotransferases: common structure and diverse functions. *Biochem. J.* 387, 281-293.

Sorre, B., Callan-Jones, A., Manneville, J. B., Nassoy, P., Joanny, J. F., Prost, J., Goud, B. and Bassereau, P. (2009). Curvature-driven lipid sorting needs proximity to a demixing point and is aided by proteins. *Proc. Natl. Acad. Sci. U. S. A* **106**, 5622-5626.

Subathra, M., Qureshi, A. and Luberto, C. (2011). Sphingomyelin synthases regulate protein trafficking and secretion. *PLoS. One.* **6**, e23644.

Tian, Y., Pate, C., Andreolotti, A., Wang, L., Tuomanen, E., Boyd, K., Claro, E. and Jackowski, S. (2008). Cytokine secretion requires phosphatidylcholine synthesis. *J. Cell Biol.* **181**, 945-957.

Ulrix, W., Swinnen, J. V., Heyns, W. and Verhoeven, G. (1998). Identification of the phosphatidic acid phosphatase type 2a isozyme as an androgen-regulated gene in the human prostatic adenocarcinoma cell line LNCaP. *J. Biol. Chem.* **273**, 4660-4665.

van Meer, G., Voelker, D. R. and Feigenson, G. W. (2008). Membrane lipids: where they are and how they behave. *Nat. Rev. Mol. Cell Biol.* **9**, 112-124.

Villani, M., Subathra, M., Im, Y. B., Choi, Y., Signorelli, P., Del, P. M. and Luberto, C. (2008). Sphingomyelin synthases regulate production of diacylglycerol at the Golgi. *Biochem. J.* **414**, 31-41.

Waggoner, D. W., Gomez-Munoz, A., Dewald, J. and Brindley, D. N. (1996). Phosphatidate phosphohydrolase catalyzes the hydrolysis of ceramide 1-phosphate, lysophosphatidate, and sphingosine 1-phosphate. *J. Biol. Chem.* **271**, 16506-16509.

White, J., Johannes, L., Mallard, F., Girod, A., Grill, S., Reinsch, S., Keller, P., Tzschaschel, B., Echard, A., Goud, B. et al. (1999). Rab6 coordinates a novel Golgi to ER retrograde transport pathway in live cells. *J. Cell Biol.* **15**, 743-760.

Yang, J. S., Gad, H., Lee, S. Y., Mironov, A., Zhang, L., Beznoussenko, G. V., Valente, C., Turacchio, G., Bonsra, A. N., Du, G. et al. (2008). A role for phosphatidic acid in COPI vesicle fission yields insights into Golgi maintenance. *Nat. Cell Biol.* **10**, 1146-1153.

Yang, J. S., Valente, C., Polishchuk, R. S., Turacchio, G., Layre, E., Moody, D. B., Leslie, C. C., Gelb, M. H., Brown, W. J., Corda, D. et al. (2011). COPI acts in both vesicular and tubular transport. *Nat. Cell Biol.* **13**, 996-1003.

Zhang, Q. X., Pilquil, C. S., Dewald, J., Berthiaume, L. G. and Brindley, D. N. (2000). Identification of structurally important domains of lipid phosphate phosphatase-1: implications for its sites of action. *Biochem. J.* **345**, 181-184.

FIGURE LEGENDS

Figure 1. Subcellular localization of LPP3 in compartments of the secretory pathway. (A). HeLa cells expressing ERGIC53-GFP stained with anti-LPP3 antibody. (B) HeLa cells treated with nocodazole (NZ) and stained with anti-LPP3 and anti-Sec32, anti-KDELr, anti-GM130 and Golgin 97 antibodies. The rightmost panels show magnifications of the nocodazole-induced ministacks for each staining condition (enlarged boxes) and graphs depicting the average fluorescence intensity profiles taken from lines traced over 30 ministacks. (C) Quantitative analysis of the results shown in B. (D) Time-lapse frames extracted from movie 1 showing the dynamic association of LPP3-GFP in the ER of COS-7 cells. Bar, 10 µm.

Figure 2. Inhibition of ERGIC tubulation by propanolol. Time series of live cells extracted from movies 2, 3 and 4. HeLa cells expressing ERGIC53-GFP were incubated at 15°C for 1 h with no addition (control) (A) or in the presence of propanolol (60 µM) for the last 5 min (B) and then shifted to 37°C. Magnifications from the indicated cell region recorded over time are shown below. (C) Initial time-point after washing propanolol in cell showed in panel B. Magnifications below show different time-points afterwards. In A and C, arrows with the same color indicate the temporal dynamics of the same ERGIC53-GFP dot-like structure. Bar, 10 µm.

Figure 3. ERGIC tubulation is inhibited in LPP3 knockdown cells. (A) Lysates from HeLa cells transfected with human LPP3-FLAG were subjected to western blot and incubated with anti-FLAG and anti-LPP3 antibodies. Lysates from these same cells as well as lysates form cells transfected for 72 h with a non-target pool of siRNAs (N-T) or with a combination of two LPP3 specific siRNAs (#6+#8) were revealed with anti-LPP3 antibodies. Equally processed LPP3 knockdown cells were transfected the last 24 h with murine LPP3-myc, and examined by western blotting with anti-LPP3 and anti-myc antibodies. Quantitative analysis of resulting LPP3 levels in the indicated transfection conditions are shown on the right; ***$p \leq 0.001$. (B) Control (mock-transfected) and LPP3-silenced HeLa cells were first incubated at 15°C for 30 min (a and c) and afterwards shifted to 37°C for 10 min (b and d), fixed and stained with anti-KDELr antibody. (C) Quantitative analysis of cells showing KDELr-stained tubules after 10 min of rewarming in control (mock-transfected), non-targeting (N-T) and LPP3 siRNAs transfected cells. *$p \leq 0.05$. (D) Control and LPP3-silenced cells were

incubated at 15°C for 30 min in the presence of DOG for the last 10 min, then rewarmed to 37°C and processed as indicated in A. Small red arrows point to representative tubular structures. (E) Quantitative analysis of results shown in D. **p ≤ 0.01, ***P ≤ 0.001. Bars, 10 µm.

Figure 4. LPP3 silencing perturbs ERGIC membrane dynamics and morphology but not ER-to-Golgi VSV-G transport. (A) Control and LPP3-silenced HeLa cells constitutively expressing VSVG-GFP were lysed at different time-points after the shift to the permissive temperature (32°C) and incubated with Endo H. Total amount of VSVG-GFP was examined by western blot with an anti-GFP antibody. The ratio (in percentage) of the amount of Endo H-resistant form to that of the total amount (Endo H-resistant/R+Endo H-sensitive/S forms) for each time-point is shown. (B) Control and LPP3-silenced HeLa cells were cotransfected overnight with ssDsRed and ERGIC53-GFP. Then, cells were incubated at 15°C for 2 h (a and b) and shifted to 37°C for 20 min (c and d). (C) Colocalization (white points in insets) of ERGIC53-GFP and ssDsRed in control (a, c, e) and LPP3-silenced (b, d, f) cells after 20 min of rewarm. (D) ERGIC53-GFP colocalizing with ssDsRed over the total ERGIC53-GFP dot-like structures. (E) ssDsRed colocalizing with ERGIC53-GFP over the total ssDsRed punctuated structures. (F) Density of ERGIC53-GFP dot-like structures. (G) Size of ERGIC53-GFP clusters; *p ≤ 0.05. Bars, 10 µm.

Figure 5. Alterations of Rab6-dependent protein transport in LPP3 knockdown cells. (A) Control and LPP3-silenced HeLa cells stably transfected with Rab6-GFP were incubated at 15°C for 1 h (a and c) and then shifted to 37°C for 10 min before fixation (b and d). The boxed areas are shown at higher magnification on the right. Arrows indicate Rab6-GFP tubular structures. (B-D) Quantitative analysis of all cytoplasmic structures (punctated and tubular; generically named particles) that contain Rab6-GFP (B), number of Rab6-GFP tubules per cell (C) and tubule length (D) in control and LPP3-silenced cells shown in (A). (E) STxB was internalized for 2 h at 37°C followed by 1 h at 15ºC and 10 min rewarm to 37°C. Cy3-STxB nuclear envelope staining appears in control (red arrows in a) but not in LPP3-silenced (c) HeLa cells expressing Rab6-GFP. Colocalization of cy3-STxB and Rab6-GFP in vesicles and tubules generated from the Golgi in control (b) and LPP3-silenced (d) cells. (F) Quantitative analysis of STxB in the ER. *p ≤ 0.05 and **p ≤ 0.01. (G) Human LPP3 knockdown cells were transfected the last 24 h of silencing (72 h) with the plasmid expressing the

murine myc-tagged LPP3 wild-type form (LPP3wt-myc). Subsequently, cells were incubated with cy3-STxB and let it to internalize following the same protocol as indicated above. Human LPP3 silenced cells expressing murine LPP3wt (asterisk) showed Golgi- and ER-like staining patterns of STxB, whereas neighboring cells not expressing mLPP3-myc only showed the Golgi-like pattern (arrow). Panels on the right are higher magnifications of indicated cells shown on left panels. Arrowheads point to STxB in the nuclear envelope. Bars, 10 µm.

Figure 6. The catalytically inactive LPP3 mutant impairs Rab6-dependent Golgi to-ER protein transport. (A) HeLa cells were co-transfected with hLPP3wt-GFP and Rab6-myc plasmids and the colocalization of both proteins analyzed by confocal microscopy. Magnified pictures below show subcellular structures co-labeled for both proteins (arrowheads). (B) HeLa cells expressing hLPP3wt-GFP with internalized STxB (see protocol indicated in Fig. 5E). Magnified pictures below show vesicular structures labeled only for LPP3 (arrows) or colabeled for LPP3 and STxB (arrowheads). (C) STxB internalized in COS-7 cells expressing hLPP3-GFP or hLPP3S197T. Below a representative example of hLPP3-GFP or LPP3S197T-GFP and cy3-STxB intensity profiles from random lines traced through the reticular cytoplasmic area. (D) Quantitative results from 5 lines per cell and 10 cells per experiment in two independent experiments. Bars, 10 µm.

Figure 7. Golgi and peri-Golgi membrane buds in LPP3-silenced cells. Swiss 3T3 cells were infected with an empty vector (control) or with LPP3 shRNA lentivirus (TCR49), fixed after 96 h of infection and processed for TEM. (A) In control cells, the Golgi exhibits an extended ribbon structure containing flat cisternae surrounded by a few peri-Golgi vesicular structures. (B-D) In LPP3 knockdown cells, Golgi stacks show slightly swollen cisternae and numerous peri-Golgi vesicular profiles that remained attached to the cisterna by a neck (outlined white ovals). Red arrows in D (which is the enlarged box outlined in C) indicate the presence of an electrondense material that corresponds to the coatomer. Bar, 200 nm.

Figure 8. Reduction of the *de novo* synthesis of DAG, TAG and major phospholipids in LPP3-silenced cells. Control and LPP3-silenced HeLa cells were labeled with [^{14}C]-acetate (A, B and C) or with [^{32}P]-orthophosphoric acid (D) for the last 24 h of the silencing protocol. Lipids were extracted, separated by TLC, and

counted for radioactivity. The labeling with [^{14}C]-acetate of DAG and TAG (A) and main phospholipids (C), but not PA (B) is reduced in LPP3-silenced cells, whereas the labeling of phosphololipids with [^{32}P]-orthophosphoric acid is similar in control and silenced cells (D). Results from a representative experiment. PE, phosphatidylethanolamine; PC, phosphatidylcholine; SM, sphingomyelin; PI, phosphatidylinositol (PI); PS, phosphatidylserine; DAG, diacylglycerol; TAG, triacylglycerol.

SUPPLEMENTARY FIGURE LEGENDS

Supplementary Figue 1. Subcellular localization of overexpressed LPP3wt-GFP in COS-7 and HeLa cells. COS-7 and HeLa cells expressing for 24 h human LPP3wt-GFP, fixed and stained for GM130 or Golgin97. Bar, 10 µm.

Supplementary Figure 2. LPP3 behaves in part as an ER-to-Golgi cycling protein. (A) Time-lapse of LPP3-GFP and VSVG-YFP fluorescence recovery after photobleaching of the Golgi area in COS-7 cells transiently transfected with LPP3-GFP or VSV-G-YFP plasmids. For VSVG-YFP experiments, cells were incubated overnight at 40°C to keep the protein accumulated at the ER. Subsequently, cells were treated with cycloheximide, shifted to 32°C for 10 min and the fluorescence at the Golgi area was bleached. Images show the recovery of the fluorescence at the Golgi after 30 min. The recovery of Golgi intensity occurs in parallel to the disappearance of the ER staining. However, after 30 min post-bleach of the Golgi area in LPP3-GFP transfected cells, the reticular fluorescence staining remains almost unchanged in comparison to that observed in the beginning of the photo-bleach. On the right, graphs depicting the rate between the Golgi and the whole cell fluorescence along the time for LPP3-GFP and VSVG-YFP. (B). Fluorescence recovery after photobleaching of the LPP3-GFP signal out of the Golgi showing after 20 min of post-bleaching the presence of LPP3-GFP again at the ER. Arrowheads indicate the staining of the nuclear envelope. Bars, 10 µm.

Supplementary Figure 3. ShRNA and lentiviral infection in Swiss 3T3 cells. (A) Cell lysates from Swiss3T3 cells mock infected (control) or infected with LPP3 shRNA lentivirus (TRC49 and TCR51) were obtained after 96 h of infection and analyzed by Western blotting with anti-LPP3 antibodies. The histogram shows the percentage of total LPP3 protein content in silenced cells compared to mock infected cells. $^{**}p \leq 0.01$ and $^{***}p \leq 0.001$.

Supplementary Figure 4. The density of KDELr particles is reduced in LPP3-depleted cells. Representative images of the KDELr staining and its quantitative analysis in control and LPP3-silenced HeLa cells. Bar, 10 µm

Supplementary Figure 5. Propanolol reduces the exit of Rab6-GFP transport carriers from the Golgi. Time series of live cells extracted from supplementary movies 4 and 5. HeLa cells stably expressing Rab6-GFP were incubated at 15°C for 1 h and then shifted to 37°C initiating time-lapse recording (left panel and time points below extracted from movie 5). Propanolol was added at the moment of rewarming cells to 37°C (right panel and time points below extracted from movie 6). Arrows point to the dynamic formation and consumption of Rab6-GFP tubules exiting from the Golgi at the indicated times after rewarming. Note that tubules formed after propanolol treatment are longer and require more time to generate vesicular carriers. Bar, 10 µm

Supplementary Figure 6. LPP3 depletion does not alter the trafficking of STxB from the plasma membrane to the Golgi. Control and LPP3-silenced HeLa cells expressing Rab6-GFP were incubated with STxB at 4°C for 15 min (a and d). After washing unbound toxin, cells were incubated at 37°C for 2 h, allowing the toxin to accumulate in the Golgi (b and e). Thereafter, cells were cooled at 15°C for 60 min. A synchronized redistribution of STxB in peripheral vesicle-like structures was observed in both cases (c and f). Bar, 10 µm.

Supplementary Figure 7. LPP3 silencing inhibits the COPI-dependent retrograde transport of STxB-KDEL. Control and LPP3 silenced Swiss 3T3 cells were incubated with STxB containing the ER-retention KDEL signal (STxB-KDEL) at 19.5°C for 3 h to block transport at the early endosomal compartment. Localization of STxB-KDEL in this compartment was analyzed using anti-EEA1 antibodies (A, B, I, J). Thereafter, cells were warmed to 37°C to induce the synchronic retrograde transport of the toxin to the ER through the Golgi complex (C-H, K-P), which was visualized with anti-giantin antibodies. After 6 h at 37°C, almost all the STxB-KDEL was already localized in the ER in control cells, whereas the majority of STxB was still retained in the Golgi in LPP3-silenced cells. The histogram shows the percentage of cells showing STxB-KDEL staining in the Golgi at 2, 4 and 6 h after the shift to 37°C. Bar, 10 µm.

Supplementary Fig. 8. Catalytically inactive LPP3 prevents the induced redistribution of Rab6 to the ER. (A) Rab6-myc subcellular localization in high overexpressed Rab6-myc cells cotransfected with LPP3wt-GFP or with the catalytically

inactive LPP3197T-GFP mutant. (B) Quantitative analysis of the different Rab6-myc redistribution patterns (ER and ER-Golgi) showed in A.

Supplementary Figure 9. Redistribution of the PKCθ-C1b domain from the Golgi to the cytosol is perturbed in LPP3-silenced cells. Control (a, b, e, f) and silenced (c, d, g, h) Swiss 3T3 cells using LPP3 shRNA lentivirus (TCR49) were transfected with GFP-tagged C1b domain of PKCθ and stained with anti-GM130 antibody to visualize the Golgi (upper panels). Bottom panels: magnifications of boxes indicated in the upper panels. The relative fluorescence intensity emitted by GFP is shown (maximum in red; intermediate in green; minimum in blue) in the Golgi. Note that the GFP-C1b intensity at the Golgi is higher in control than in LPP3-silenced cells. Images are representative of two different experiments. Bar, 10 µm.

Supplementary movies

Movie 1. LPP3wt-GFP dynamics in the ER of COS-7 cells

Movie 2. ERGIC53-GFP dynamics in control HeLa cells

Movie 3. ERGIC53-GFP dynamics in propranolol-treated HeLa cells

Movie 4. ERGIC53-GFP dynamics after propranolol wash-out

Movie 5. Rab6-GFP dynamics in control HeLa cells

Movie 6. Rab6-GFP dynamics in propranolol-treated HeLa cells

SUPPLEMENTARY MATERIAL AND METHODS

Antibodies and plasmids

Rabbit polyclonal antibodies against LPP3 used for immunocytochemistry were generated to the 223-235aa sequence of the human protein (Alderton et al., 2001). Antibodies used for Western blotting were provided by H. Kanoh (Sapporo Medical University School of Medicine, Japan). Mouse monoclonal antibodies to KDEL receptor were purchased from Calbiochem, BD Transduction Laboratories (San José, CA, USA). Mouse monoclonal antibodies to GM130 and myc, and rabbit polyclonal antibodies to FLAG were purchase from Sigma (St. Louis, MO, USA). Mouse monoclonal antibody to Golgin97 and rabbit polyclonal antibody to GFP were purchased from Molecular Probes (Paisley, United Kingdom). Secondary antibodies ($F(ab')_2$ fragments) conjugated to Cy3- or Alexa-488 were from Jackson InmunoResearch Laboratories (West Grove, PA, USA). Secondary antibodies conjugated to HRP were from Promega (Madison, WI, USA).

Plasmids: LPP3wt-GFP and LPP3S197T-GFP were provided by H. Kanoh (Medical University School of Medicine, Sapporo, Japan), Rab6-myc was from B. Goud (Institute Curie, Paris, France), GFP-C1 domain-PKCθ was from I. Mérida (CSIC, Madrid, Spain), and ERGIC53-GFP and ssDsRed were from H.-P. Hauri (Biozentrum, University of Basel, Basel, Switzerland). Plasmids encoding mouse LPP3wt-myc and human Gb3 synthase were purchased from Origene (Rockville, MD, USA). The second-generation lentivirus packaging (psPAX2) and envelope plasmids (pMD2.G) were provided by R.M. Rios (Cabimer, Sevilla, Spain). Cy3-conjugated wild type Shiga toxin B subunit (STxB) and STxB coupled to the KDEL sequence (STxB-KDEL) were provided by L. Johannes (Institut Curie, Paris, France).

Chemicals and reagents. Brefeldin A (BFA) and 2-dioctanoyl-sn-glycerol (DOG) were purchased from Sigma (St. Louis, MO, USA), propanolol and nocodazole were from Calbiochem (Darmstadt, Germany). Endoglycosidase H (Endo H) was purchased from New England Biolabs (Beverly, MA), and [^{14}C]acetate and [^{32}P]orthophosphoric acid were from PerkinElmer Life Sciences (Waltham, MA, USA). Unless otherwise stated, all other chemicals were from Sigma or Calbiochem.

Cell lines and cell culture conditions. HeLa cells stably expressing Rab6-GFP were provided by B. Goud (Institut Curie, Paris, France). HeLa cells stably expressing VSVG-GFP were provided by V. Malhotra (Center of Regulatory Genomics, Barcelona, Spain). HeLa, COS-7, Swiss 3T3, and 293T cells were cultured in DMEM (Invitrogen, Paisley, United Kingdom) containing 10% of fetal calf serum (FCS; GIBCO/BRL Invitrogen, Paisley, United Kingdom) and supplemented with sodium pyruvate (1 mM), glutamine (2 mM), penicillin (100 U/ml), and streptomycin (100 µg/ml). Cells were grown in a humidified incubator in 5% CO_2 at 37°C. Expression of stably transfected HeLa Rab6-GFP and HeLa VSV-GFP cells was maintained by adding geniticin (500 µg/mL) to the culture medium. For the temperature experiments, cells were cultured in a temperature-controlled incubator at 15°C for different periods of time. Where indicated, cells were treated with nocodazole (NZ, 30 µM), propanolol (60 or 100 µM), DOG (3 µM), or BFA (2 µg/mL) for the indicated times.

FRAP and iFRAP experiments.

Fluorescence recovery after photobleaching (FRAP) experiments were performed using the Leica confocal mentioned above equipped with an incubation system with temperature and CO_2 control. COS-7 cells were seeded to 35 mm plate (Nunc, Roskilde, Denmark) containing a glass coverslip of 22 mm (Micro cover glass; Electron Microscopy Sciences, Fort Washington, PA). 24h after seeding COS-7 cells were transfected with LPP3-GFP and VSVG-YFP. In the case of VSV-G transfected cells were incubated at 40°C to accumulate the protein at the ER overnight. For FRAP experiments 24 h after transfection, the glass coverslip was mounted in the video confocal chamber, keeping the cells at 33°C. For FRAP experiments, the whole Golgi area was photobleached using 40 scans with the 488 nm laser line at full power. Subsequent images were taken every 0.657 seconds using x63 oil immersion objective lens (numerical aperture, 1.32), 488 nm laser line and the confocal pinhole set at 5 Airy units to minimize changes in fluorescence efficiency attributable to proteins moving away from the plane of focus. Recovery of the Golgi-associated intensity was monitored for about 30 min.

To evaluate the results of photobleaching experiments, the observed fluorescence equilibration in the bleached region (the Golgi complex) was quantified using the Image Processing Leica Confocal Software. Background fluorescence was measured in a random fieldoutside of cells. All experiments were background subtracted, corrected

and normalized using the equation described below. For each time point the relative recovery of total fluorescent intensity in the bleached Golgi region was calculated as: $I_{[t]}$ = (I $Golgi_{[tx]}$ / I $Golgi_{[t0]}$) x (I $Cytoplasm_{[t0]}$ / I $Cytoplasm_{[tx]}$) x 100, where I $Golgi_{[tx]}$ and I $Cytoplasm_{[tx]}$ are the average fluorescence intensities of the bleached (Golgi) and unbleached (Cytoplasm) regions at the time-point x, and I $Golgi_{[t0]}$ and I $Cytoplasm_{[t0]}$ are the average intensities of the corresponding areas before the Golgi bleach.

For iFRAP experiments, after about 24h of transfection with LPP3wt-GFP, COS-7 cells were treated with cycloheximide (Sigma, St.Louis, MO, USA) at 0,1 mg/mL just before performing photobleach of the fluorescence out of the Golgi by 80 scans with the 488 nm laser line at full power. Afterwards, images were collected with a 63× oil immersion objective lens (numerical aperture, 1.32, pinhole set at 1 Airy units) applying a 6x zoom to visualize the endoplasmic reticulum fluorescence recovery along time. Images were collected every 5min. for a 20 min. period.

Image processing

All the images were analyzed using the freeware ImageJ version 1.33 by Wayne Rasband (NIH, Bethesda, USA). Briefly, the total number of KDELr and Rab6-GFP tubular structures per cell was the result of summing the tubules counted in each slice. The density of ERGIC53-GFP and KDELr dot-like structures was calculated setting an arbitrary threshold on the Z projection of different slices and making a ratio between the number vesicles and the cell area (in both cases excluding the Golgi). The size of ERGIC53-GFP dot-like structures was calculated converting the average area in pixels of individual vesicles to their diameter (in nm). Rab6-GFP number of tubular and globular transport carriers was calculated as indicated above by counting the number of structures between 5 and 200 pixels. The length of Rab6-GFP tubules was calculated from the Z projection of different slices by measuring the area in pixels of drawn lines connecting the extremes of each tubule. The method to quantify colocalization between the different markers was the following: the cell area was delineated setting up a threshold for each of the markers assessed. Afterwards, colocalization analysis was performed using the ImageJ plugin named “colocalization highlighter”, considering “colocalization” when the ratio of fluorescence intensities between red and green channels was above 0.5. Those pixels above the threshold in which this ratio is accomplished appear in a binary image color as white. Thereafter, a ratio between the number of pixels of one channel that colocalizes with the marker in the other channel

and the total number of pixels above the threshold measured for each of the channels was obtained. To quantify colocalization between LPP3wt-GFP and LPP3S197T-GFP with the STxB-cy3 subunit at the ER, the fluorescence intensity profiles of each marker were obtained tracing lines randomly along the reticular staining of LPP3wt and S197T. For each pixel we calculated the difference between the LPP3wt/S197T-GFP and StxB-cy3 intensities.

Protein transport assays.

For the ssDsRed transport assay, HeLa cells were cotransfected with plasmids encoding ssDsRed and ERGIC53-GFP. After 17-20 h of expression, anterograde traffic from the ERGIC was blocked by incubating cells at 15°C for 2h. Thereafter, cells were warmed to 37°C and incubated at 37ºC for 20 min to allow ssDsRed transport to the Golgi.

For the VSVG-GFP Endo-H resistance acquisition transport assay, HeLa cells stably expressing VSV-G-GFP were incubated the last 24 h of silencing at 40°C. Cycloheximide was added to a final concentration of 100 ng/mL, and then cells were shifted to 32°C to allow transport. Cell lysates at different time-points after the temperature shift were obtained solubilizing pellets in 0.5% SDS and 1% 2-mercaptoethanol (0.1 ml/35-mm dish), and heated to 100°C. Twenty µg of protein from each lysate was digested with Endo-H according to the manufacturer's protocol and subjected to SDS-PAGE on 8% gels. VSVG-GFP was detected by immunoblotting with an anti-GFP antibody.

For the wild-type Shiga toxin B fragment (STxB) transport assay, we used two cell lines: HeLa cells (wild type or stably expressing Rab6-GFP) and COS-7 cells co-transfected with either LPP3wt-GFP or LPP3S197T-GFP together with a plasmid encoding the enzyme Gb3 synthase. Transfection with the Gb3 synthase in COS-7 cells was necessary as this cell line express very low levels of the STxB receptor Gb3. Briefly, cells were first incubated for 15 min in DMEM in the presence of 0.5 µg/mL of Cy3-STxB. Subsequently, the unbound Shiga toxin was removed by three washes with ice-cold PBS. Thereafter, fresh DMEM was added and cells were incubated at 37°C for 2 h to accumulate internalized STxB in the Golgi. Next, retrograde transport from the Golgi to the ER was synchronized incubating cells for 1 h at 15°C, after which STxB arrival in the ER was allowed by shifting cells to 37°C for 10 min (in HeLa) or 1h (in COS-7).

For the Shiga toxin B subunit containing the KDEL sequence (STxB-KDEL) transport assay, Swiss 3T3 cells were first incubated with Cy3-ST-B-KDEL (4 µg/mL) for 45 min at 4°C and, subsequently, the unbound toxin was removed by three washes with ice-cold PBS. Thereafter, cells were incubated with DMEM at 19°C for 2 h to accumulate the internalized STxB-KDEL in early/recycling endosomes. Next, cells were shifted to 37ºC. In all transport experiments cells were fixed in PFA (4% in PBS) at the indicated times.

Statistics. Unless stated otherwise, data are presented as mean ± s.e.m. of at least three independent experiments. Statistical analysis was performed with either a paired Student's *t* test or ANOVA one-way followed by Tukey's multiple comparison test. For statistical computation and estimation of significance, we used the online software GraphPad (San Diego, CA; www.graphpad.com).

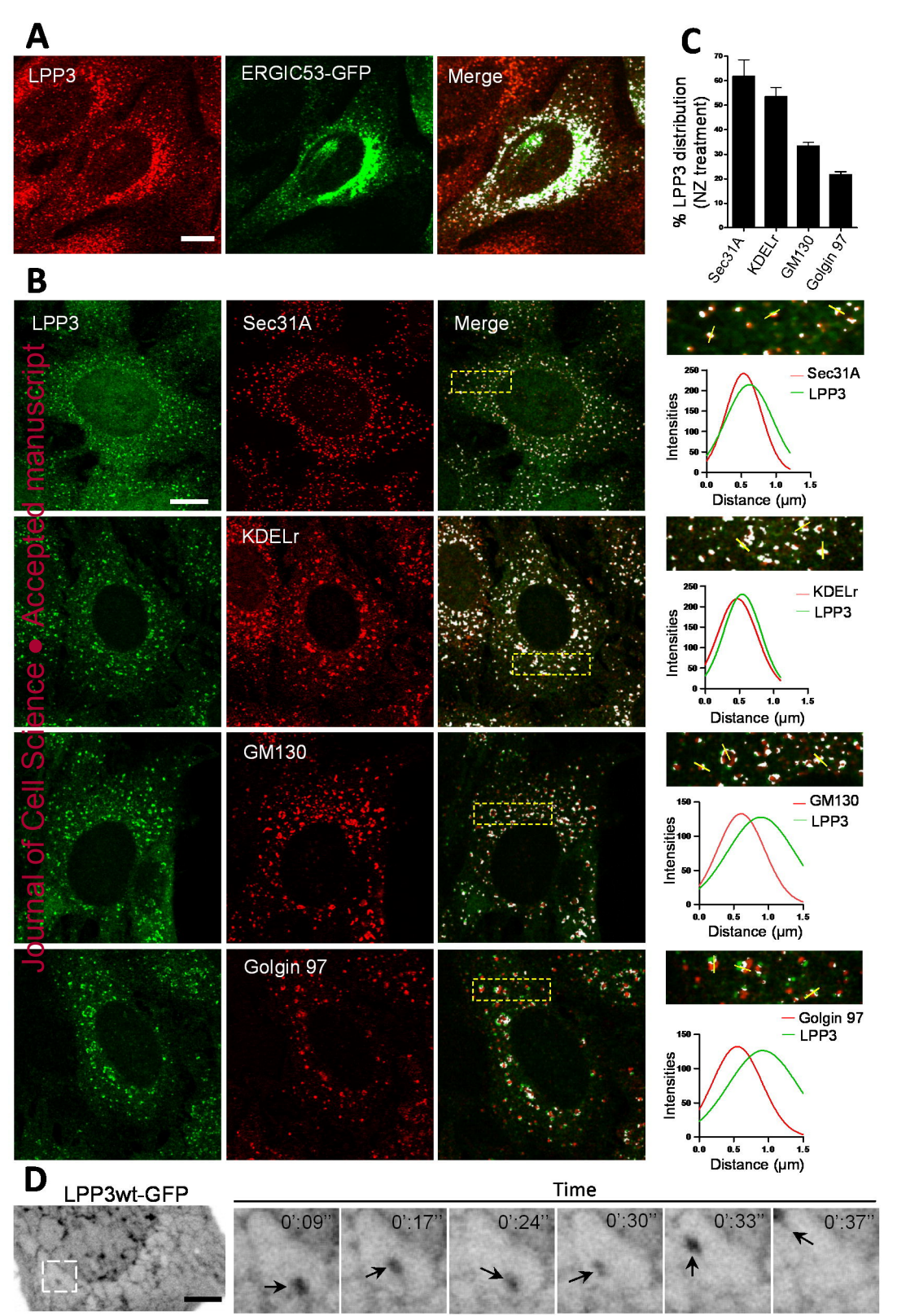
A
LPP3
ERGIC53-GFP
Merge
C
% LPP3 distribution (NZ treatment)
Sec31A
KDELr
GM130
Golgin 97
B
LPP3
Sec31A
Merge
KDELr
GM130
Golgin 97
Intensities
Distance (µm)
Journal of Cell Science • Accepted manuscript
D
LPP3wt-GFP
Time
0':09''
0':17''
0':24''
0':30''
0':33''
0':37''